Mechanistic insights into the synergistic activation of the RXR–PXR heterodimer by endocrine disruptor mixtures

Vanessa Delfosse[a,1], Tiphaine Huet[a,1], Deborah Harrus[a,1], Meritxell Granell[a,1], Maxime Bourguet[b,1], Caroline Gardia-Parège[c], Barbara Chiavarina[c], Marina Grimaldi[c], Sébastien Le Mével[d], Pauline Blanc[a], David Huang[a], Jakub Gruszczyk[a], Barbara Demeneix[d], Sarah Cianférani[b], Jean-Baptiste Fini[d,2], Patrick Balaguer[c,2], and William Bourguet[a,2]

[a]Centre de Biologie Structurale, INSERM, CNRS, Université de Montpellier, Montpellier, France; [b]Laboratoire de Spectrométrie de Masse BioOrganique, Université de Strasbourg, CNRS, Institut Pluridisciplinaire Hubert Curien, Unité Mixte de Recherche 7178, 67000 Strasbourg, France; [c]Institut de Recherche en Cancérologie de Montpellier, INSERM, Institut Régional du Cancer de Montpellier, Université de Montpellier, Montpellier, France; and [d]Muséum National d'Histoire Naturelle, Laboratoire Physiologie Moléculaire et Adaptation, CNRS Unité Mixte de Recherche 7221, Paris, France

Edited by Mitchell A. Lazar, University of Pennsylvania, Philadelphia, PA, and approved November 23, 2020 (received for review October 8, 2020)

Humans are chronically exposed to mixtures of xenobiotics referred to as endocrine-disrupting chemicals (EDCs). A vast body of literature links exposure to these chemicals with increased incidences of reproductive, metabolic, or neurological disorders. Moreover, recent data demonstrate that, when used in combination, chemicals have outcomes that cannot be predicted from their individual behavior. In its heterodimeric form with the retinoid X receptor (RXR), the pregnane X receptor (PXR) plays an essential role in controlling the mammalian xenobiotic response and mediates both beneficial and detrimental effects. Our previous work shed light on a mechanism by which a binary mixture of xenobiotics activates PXR in a synergistic fashion. Structural analysis revealed that mutual stabilization of the compounds within the ligand-binding pocket of PXR accounts for the enhancement of their binding affinity. In order to identify and characterize additional active mixtures, we combined a set of cell-based, biophysical, structural, and in vivo approaches. Our study reveals features that confirm the binding promiscuity of this receptor and its ability to accommodate bipartite ligands. We reveal previously unidentified binding mechanisms involving dynamic structural transitions and covalent coupling and report four binary mixtures eliciting graded synergistic activities. Last, we demonstrate that the robust activity obtained with two synergizing PXR ligands can be enhanced further in the presence of RXR environmental ligands. Our study reveals insights as to how low-dose EDC mixtures may alter physiology through interaction with RXR–PXR and potentially several other nuclear receptor heterodimers.

cocktail effect | endocrine disruptor | low dose | synergy | mixture

The human xenobiotic response is mediated primarily by the nuclear receptor (NR) 1I2 (pregnane X receptor, PXR), a unique sensor activated by a large array of compounds (1). It has been identified by the American Environmental Protection Agency ToxCast's program as a major front-line target of chemicals. PXR heterodimerizes with the retinoid X receptors (RXRα, β, γ; NR2B1–3) and plays a critical protective role in regulating the expression of detoxifying enzymes (e.g., cytochrome CYP3A4) and transporters (e.g., ATP-dependent efflux pump MDR1) that drive liver and gastrointestinal metabolism, as well as clearance of many exogenous and endogenous substances such as drugs, environmental pollutants, food components, or hormones. However, sustained activation of PXR is also known to provoke undesirable effects, including drug–drug interactions, resistance to cancer therapy, formation and accumulation of toxic intermediates, or defects in the homeostasis of endogenous compounds like steroid hormones or bile acids (2, 3). In addition, PXR is also expressed in various cancerous tissues (e.g., colon adenocarcinoma, hepatocellular carcinoma), where its activation has been linked to increased cell proliferation and tumor aggressiveness (4). The interaction of PXR with xenobiotics has also been linked to an increased risk of cardiovascular (5) and metabolic (6) diseases.

Unlike most NRs that bind few ligands with structural homologies, PXR interacts with a large number of compounds that differ greatly in size and chemical structures (7). For example, PXR binds to and is activated by high molecular weight compounds such as the anticancer drug paclitaxel (854 Da) and the antibiotic rifampicin (823 Da), or smaller ones like the insecticide fipronil (FIP; 437 Da), the natural hormone estradiol (E2; 272 Da), and the plasticizer bisphenol-A (228 Da), to cite but a few. Moreover, we have shown previously that the ligand-binding pocket (LBP) of PXR can accommodate two different compounds simultaneously and that this cobinding leads to dramatic

Significance

Many environmental pollutants act as endocrine disruptors that interfere with normal endocrine regulation and promote adverse effects in humans. As a major target of xenobiotics, the pregnane X receptor (PXR) is known to play opposite roles by both facilitating their clearance and mediating their toxic effects. Here, we use structural and functional approaches to describe two converging mechanisms leading to a robust synergistic stimulation of the PXR pathway by mixtures of three chemicals exhibiting very low efficacy when administered separately. This "cocktail effect" relies on two cooperative binding processes that enhance both ligand binding affinity and recruitment of transcriptional coactivators. Our findings show how chemical mixtures may alter physiology and homeostasis at concentrations where individual components are considered safe.

Author contributions: P. Balaguer and W.B. designed research; V.D., T.H., D. Harrus, M. Granell, M.B., C.G.-P., B.C., M. Grimaldi, S.L.M., J.G., B.D., S.C., J.-B.F., and P. Balaguer performed research; P. Blanc and D. Huang contributed new reagents/analytic tools; V.D., T.H., D. Harrus, M. Granell, M.B., C.G.-P., B.C., M. Grimaldi, S.L.M., J.G., B.D., S.C., J.-B.F., P. Balaguer, and W.B. analyzed data; and W.B. wrote the paper.

The authors declare no competing interest.

This article is a PNAS Direct Submission.

[1]V.D., T.H., D.H., M.G., and M.B. contributed equally to this work.

[2]To whom correspondence may be addressed. Email: fini@mnhn.fr, patrick.balaguer@inserm.fr, or bourguet@cbs.cnrs.fr.

This article contains supporting information online at https://www.pnas.org/lookup/suppl/doi:10.1073/pnas.2020551118/-/DCSupplemental.

Published December 28, 2020.

changes in the activity of the ligands bound (8). Through extensive functional and structural analyses, we demonstrated that the pharmaceutical 17α-ethinylestradiol (EE2) and the organochlorine pesticide *trans*-Nonachlor (TNC) bind to PXR in a cooperative manner, stabilize each other within its LBP, and synergistically activate the receptor. Remarkably, biophysical characterization revealed that, when used as a binary mixture, EE2 and TNC bind to PXR with an up to 100-fold greater binding affinity than those of the individual compounds. As a consequence, a substantial expression of the PXR endogenous target gene *CYP3A4* could be observed at concentrations where single chemicals displayed no activity. This study provided a mechanistic explanation and a proof of concept for the "cocktail" or "mixture" effect where inactive chemicals can actually combine within the confined environment of a receptor LBP to form a potent supramolecular ligand. It added to the demonstrations of additive effects on signaling pathways shown by Kortenkamp and others (9–12).

Based on the observation of EE2 and TNC cobinding, we reasoned that small (<500 Da) and chemically unrelated compounds could bind to different subpockets and fill a limited portion of the PXR LBP, thereby leaving an empty volume available for accommodating a second substance. Here, we report on the structural and functional characterization of the binding mode of an eclectic subset of known PXR ligands that reveals unforeseen interaction mechanisms and confirms compound-specific partial occupancies of the LBP. We then generated binary mixtures by mixing compounds with compatible binding modes and found composite ligands displaying different degrees of synergistic activities in vitro and in vivo. Crystallographic analysis revealed details of their binding mechanisms and how individual components may adjust their own binding mode in the presence of a cobinder. Additionally, we showed by cell-based and biophysical assays that tributyltin (TBT), a well-characterized RXR environmental ligand, further potentiates the synergistic activity of EE2 and TNC by increasing the affinity of the RXR–PXR heterodimer for transcriptional coactivators. Our work provides biochemical, structural, and functional data showing various ways by which mixtures of endocrine-disrupting chemicals (EDCs) to which we are constantly exposed can disturb cell signaling at doses where individual components are assumed to be innocuous.

Results and Discussion

Structural and Functional Characterization of PXR Environmental Ligands. From the vast ensemble of compounds acting as PXR ligands, we selected a subset of 13 chemicals with molecular weights below 500 Da and exhibiting a large diversity in their chemical structures (*SI Appendix*, Fig. S1). We were able to solve the crystal structures of PXR ligand-binding domain (LBD) in complex with nine of these compounds, namely the pesticides FIP, pretilachlor (PRE), oxadiazon (OXA), endosulfan (END), and *cis*-chlordane (CC); the antifungal clotrimazole (CLO); the biocide TBT; the phytoestrogen ferutinin (FER); and the mycotoxin α-zearalanol (ZEA). However, we failed to obtain crystals or unambiguous electron densities for the pesticides heptachlor endoepoxide (HEP), fenvalerate, and toxaphene and the detergent 4-tert-octylphenol. Data collection and refinement statistics are summarized in *SI Appendix*, Table S1. In parallel, we monitored the agonistic potential of these compounds using the stably transfected HG5LN GAL4-PXR-LBD reporter cell line (8). The data reported in Fig. 1*A* and *SI Appendix*, Table S2, show half-maximal effective concentrations (EC_{50}s) ranging from 0.5 μM to 15 μM, with PRE and OXA acting as the most potent PXR agonists and CC or HEP being the least active.

The structures display the canonical active conformation of the LBD of NRs, with the C-terminal helix H12 (also termed AF-2 or activation helix) capping the LBP (*SI Appendix*, Fig. S2*A*), and compounds could be precisely placed in their respective electron density (*SI Appendix*, Fig. S2*B*), revealing different binding modes and cavity occupancies. We first observed that PXR contains an aromatic cage deeply buried at the bottom of the LBP made up of F288, W299, and Y306 that trap ligands through their most hydrophobic/aromatic moieties. This subpocket delineated by helix H5 and the β-sheet S3/S4 is involved in π-stacking, π-halogen, and/or C–H/π interactions (*SI Appendix*, Fig. S3) and constitutes the major anchoring point for END, CLO, ZEA, CC, and, to some extent, FER (Fig. 2 *A*–*E*). Additional contacts between these compounds and the LBP encompass van der Waals interactions with surrounding hydrophobic residues and essentially display no hydrogen bonding, except for FER, whose phenolic side chain extends outside the aromatic cage and forms a hydrogen bond with the E321 side chain in the loop linking H6 and H7 (Fig. 2*E*, red dashes). When compared to the unliganded form, only a few side-chain reorientations are necessary to accommodate the compounds that make no direct interaction with the activation helix H12 located on the other side of the pocket (Fig. 2 *A*–*E*). Note that this mechanism of interaction is reminiscent of that previously observed for TNC (8), suggesting a common binding mode for organochlorine pesticides that leaves vacant a significant portion of the LBP delineated by helices H3, H11, and H12.

PRE and TBT display unusual binding mechanisms, with the presence of two copies of each compound in the LBP, one or two of them covalently linked to a cysteine residue (Fig. 2 *F* and *G*). Covalent interactions were confirmed by mass spectrometry (MS) under denaturing conditions (*SI Appendix*, Fig. S4). The structures reveal that one molecule of PRE is covalently linked to C207 while the second docks between the first molecule and the aromatic cage in a noncovalent manner (Fig. 2*F*). In contrast, the two TBT molecules are bound in a face-to-face fashion through covalent bonds with C207 and C284, respectively (Fig. 2*G*). Covalent coupling occurs between the sulfur atom of cysteine residues and either the tin atom of TBT or the carbon atom of the acetamide moiety of PRE (*SI Appendix*, Fig. S4). C284 resides in the middle of helix H5 and points toward the ligand-binding cavity, whereas C207 is located in a loop following helix H2′ in the TBT and PRE structures (Fig. 2 *F* and *G*). However, in other structures, including that of unliganded (apo) PXR, H2′ is one α-helical turn longer, so C207 lies in H2′ and points outside the LBP (*SI Appendix*, Fig. S5). Ensemble refinement of several PXR LBD structures using Phenix (13) revealed that the C-terminal part of H2′ is highly flexible and easily unfolds (*SI Appendix*, Fig. S6). The dynamics of the resulting loop allow C207 to explore a vast ensemble of spatial positions that facilitate coupling reactions with the chemically reactive moieties frequently present in bioactive compounds such as pesticides (Movie S1). Again, no interaction is observed between TBT or PRE and the AF-2 helix (Fig. 2 *F* and *G*).

The structures with OXA and FIP showed that the two compounds mostly overlap and occupy a subpocket perpendicular to helix H3 and extending from H12 to the aromatic cage, leaving a volume corresponding to the binding site of the covalently bound PRE molecule empty (Fig. 2 *H* and *I*). While the interaction of OXA with PXR relies essentially on networks of halogen bonds and van der Waals interactions with LBP residues, a continuous electron density between C284 and FIP strongly suggested a covalent coupling (*SI Appendix*, Fig. S2*B*). Intriguingly, while the two ligands reside in a similar region of the LBP, they display quite different EC_{50}s (Fig. 1*A* and *SI Appendix*, Table S2). This could be explained by the larger size of FIP that might be too sterically constrained within its binding site, as suggested by the significant shift of the aromatic cage residue Y306 toward the solvent compared to its position in other PXR structures. A short residence time of FIP within the LBP could also explain why a covalent coupling is not observed by MS (short incubation time

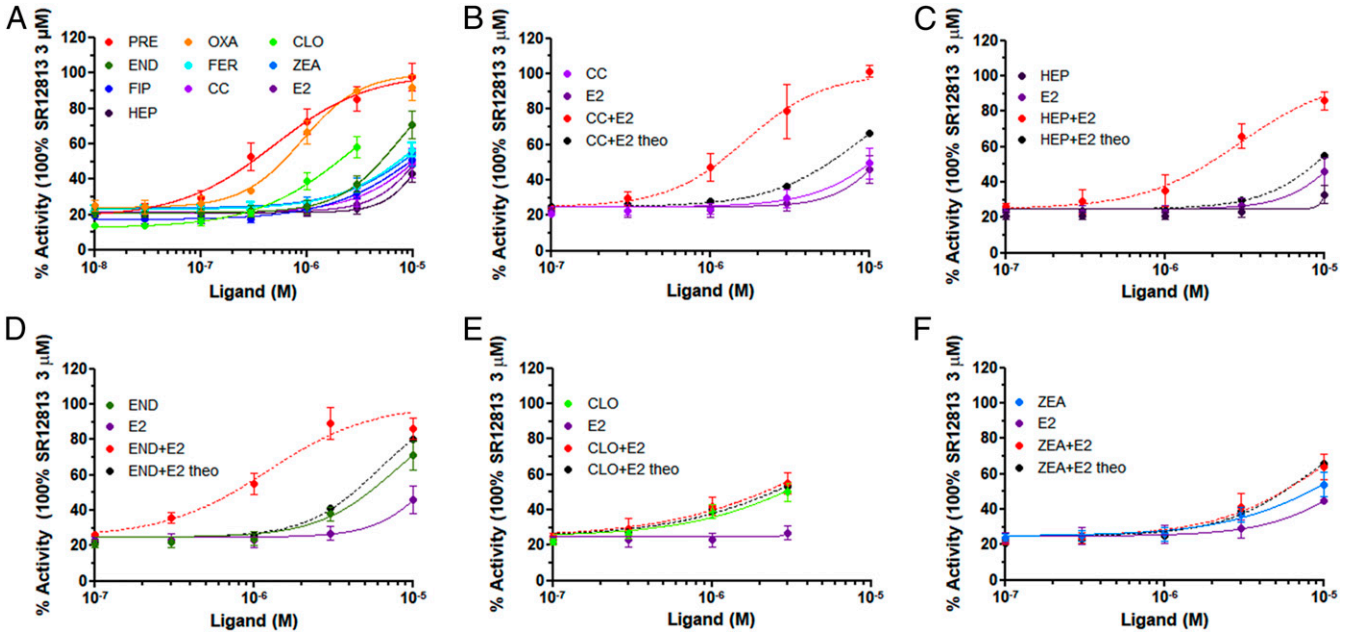

Fig. 1. Compound activity in transactivation assays using the HG5LN GAL4-PXR-LBD cell line. (*A*) Cells were exposed to different concentrations of test compounds. Assays were performed in quadruplicate in at least three independent experiments, and data are expressed as mean (±SEM). Note that, because of toxicity issues, CLO could not be used at concentrations above 3 μM. (*B–F*) Cells were exposed to compounds in binary mixtures as indicated. Black dashed lines represent the theoretical activation curves obtained for the additive combination of individual compound activities calculated using the Bliss independence model (20). Assays were performed in quadruplicate in at least three independent experiments, and data are expressed as mean (±SEM).

of 1 h), whereas it can be seen in the crystal structure, where the ligand and the receptor are coincubated for several days during the crystallization process.

As a whole, this crystallographic analysis on a limited set of chemically and structurally unrelated compounds reveals a variety of binding mechanisms and pocket occupancies. Together

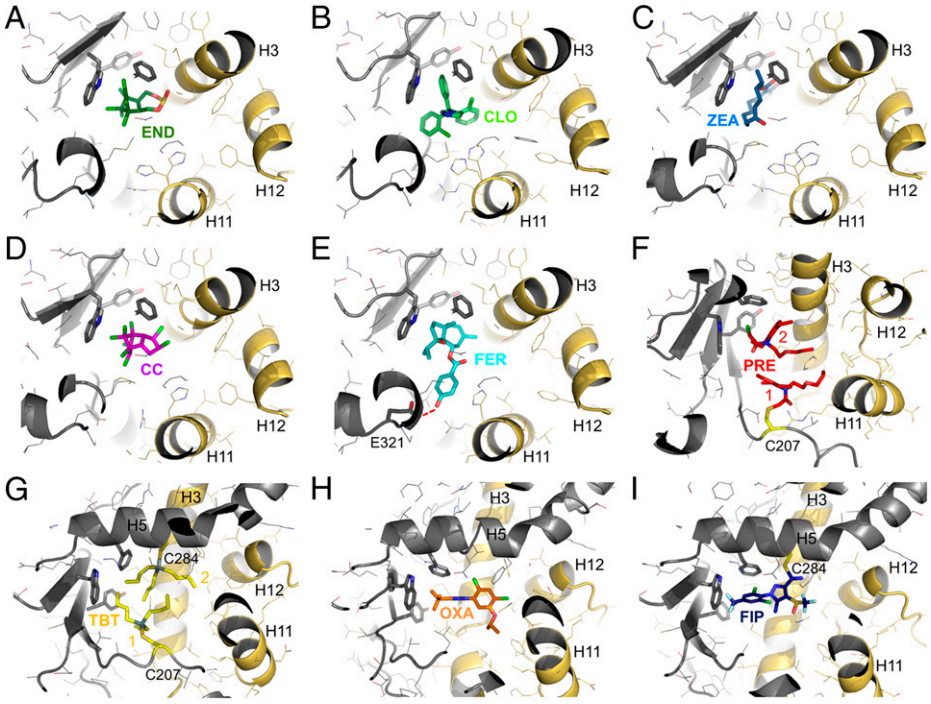

Fig. 2. Chemicals bind to PXR with varied binding mechanisms and pocket occupancies. (*A–I*) Close-up view of the LBP of PXR bound to the various test compounds. The chemicals (color code for carbon atoms as in Fig. 1*A*) and residues belonging to the aromatic cage (gray) are shown as sticks. Other residues are displayed as lines. Oxygen, nitrogen, sulfur, and chlorine atoms are colored in red, blue, yellow, and green, respectively. Residues and secondary structural elements discussed in the text are labeled.

with previously reported data, this study allowed us to delineate four PXR LBP subpockets which serve as primary binding sites for four groups of chemicals (Fig. 3). More specifically, these distinct parts of the LBP can be defined as: 1) the organochlorine pesticides' (ligand group 1) anchoring site in the aromatic cage region involving H3, H5, H7, and the β-strands S3 and S4; 2) the FIP/OXA (ligand group 2) interaction site close to helix H3 and extending from H12 to the β-sheet S3/S4; and 3) the binding site of PRE and TBT (ligand group 3) covalently bound to C207 comprising the C-terminal part of H2′ and the following variable loop, the β-strands S1 and S4 and helix H11. As shown in *SI Appendix*, Fig. S7*A*, the fourth subpocket corresponds to the previously identified binding site of steroidal ligands (ligand group 4), which is delimited by helices H2′, H3, H11, and H12 (8, 14). In contrast with our aforementioned structures, the majority of the 20 nonredundant complex structures of PXR in the Protein Data Bank (PDB) show ligands with a more central position in the LBP, mainly extending from subpocket 1 to subpocket 4 (e.g., SR12813, *SI Appendix*, Fig. S8*A*; garcinoic acid, *SI Appendix*, Fig. S8*B*). Besides, rifampicin is the only one ligand which occupies almost all of the LBP (*SI Appendix*, Fig. S8*C*), thus covering the four groups defined in this study. However, few ligands are more specifically bound to one of the four subsites (e.g., a benzothiazine in 3, *SI Appendix*, Fig. S8*D*; the HIV-1 integrase and $S1P_1$ inhibitors in 1, *SI Appendix*, Fig. S8 *E* and *F*; the P2X4 and HIV reverse-transcriptase inhibitors in 2, *SI Appendix*, Fig. S8 *G* and *H*). Finally, all ligands except estrogens of group 4 established contacts with the aromatic cage of subpocket 1 through π-stacking or C–H/π interactions, and half of them occupy at least subpocket 2 also. Therefore, subsites 3 and 4 are the least occupied.

Graded Synergistic Activity of Binary Mixtures. Based on this structural knowledge, we generated binary mixtures so as to identify new cobinders that could activate PXR in a synergistic fashion. We mixed compounds with compatible binding modes (Fig. 3) such as, for instance, organochlorine pesticides (ligand group 1) with steroidal ligands (ligand group 4) and PRE (from group 3) with ligands of groups 1 or 2 (FIP/OXA), and monitored the activity of these two-component mixtures using the HG5LN GAL4-PXR-LBD reporter cell line. Compared to the data obtained with individual ligands, most combinations exhibited additive effects, but some of them produced a synergistic activation of PXR (*SI Appendix*, Table S3). Notably, we observed that the synergistic potential of a given compound varied according to the partner ligand. For instance, we noticed a clear graded synergistic activation of PXR by combinations containing the natural hormone E2 as the common component and various ligands of group 1. In order to gain more insight into the molecular determinants of the synergistic activation of PXR by composite ligands, we proceeded further with the structural and functional characterization of these mixtures. Using the HG5LN GAL4-PXR-LBD reporter cell line, we found that the E2/CC mix displayed the best synergy factor (SF; 5.3), followed by E2/END (SF = 4.9) and E2/HEP (SF = 4.2), whereas E2/CLO (SF = 1.1) and E2/ZEA (SF = 1.0) showed very little or no synergism (Fig. 1 *B*–*F*). Note that the first described synergistic mixture EE2/TNC had an SF of 7.4 (8).

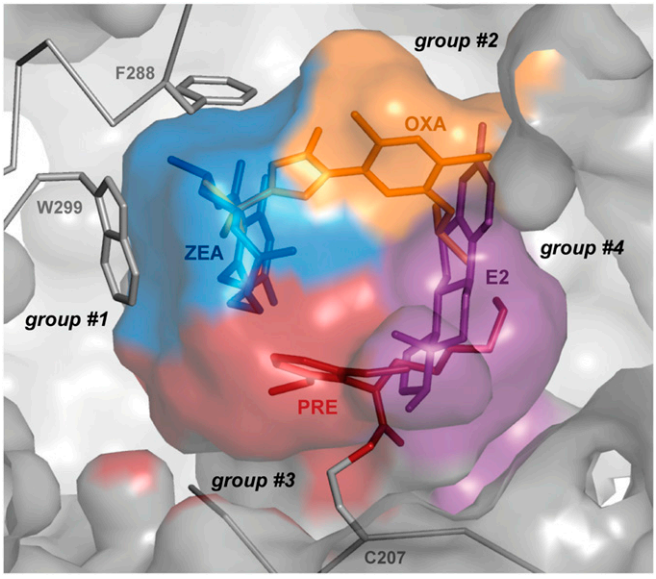

Fig. 3. Differential occupancy of the PXR LBP. The four PXR LBP subpockets defined in this study are displayed and labeled. One compound representative of each group is shown within its subpocket. Both the ligands and their pockets are colored following the code used in Fig. 1*A*.

The interaction of PXR with the chemicals either alone or in combinations was then characterized by using electrospray ionization (ESI) MS under native conditions. Analyzed separately, CLO, TNC, CC, and END bound essentially to PXR in a 1:1 molar ratio, while EE2, E2, HEP, and ZEA were found to interact with the receptor with 1:1 and 1:2 binding stoichiometries (possibly 1:3 and more for ZEA; *SI Appendix*, Fig. S9). Note, however, that nonspecific binding outside the LBP may account for the detection of ternary and quaternary complexes, as only one molecule of EE2, E2, HEP, and ZEA bound to the LBP of PXR could be identified in the corresponding crystal structures (refs. 8, 14 and this work). We then analyzed PXR in the presence of the six corresponding binary mixtures. Incubation with the EE2/TNC, E2/CC, E2/HEP, and E2/END mixtures resulted in the formation of predominant ternary complexes corresponding to PXR interacting with E2 and CC, HEP, or END, or with EE2 and TNC, in a 1:1:1 molar ratio, indicative of a greater binding affinity of the mixes compared to individual compounds (Fig. 4). In contrast, coincubation with E2 and CLO led to a slightly higher amount of 1:1 CLO-bound PXR species, suggesting an absence of binding cooperativity for the E2/CLO mixture. Last, the binding affinity of ZEA was significantly decreased in the presence of E2, as shown by the predominance of the ZEA-bound over the doubly bound species. Together, these native ESI-MS data confirmed that the LBP of PXR can accommodate two ligands simultaneously and that cobinding modifies positively or negatively the binding characteristics of each compound.

We next examined the effect of the compounds alone or in combination in an in vivo model featuring a transgenic line of *Xenopus laevis*, which expresses the green fluorescent protein (GFP) under the control of the LBD of PXR fused to the DNA-binding domain of the yeast transcription factor GAL4 (GAL4-PXR-LBD). Due to toxicity issues, only E2, EE2, TNC, END, and CC could be analyzed. As expected, injection of the reference PXR agonist SR12813 in skeletal muscle induced a strong induction of GFP, whereas treatment with each test compound alone led to little or no enhancement of the reporter gene expression relative to the control experiment (Fig. 5). However, in comparison with the ligands used alone, cotreatment with EE2 and TNC yielded much stronger activation of PXR, as revealed by the induction of GFP to a level comparable to that obtained with SR12813. In association with E2, CC and END also produced a synergistic response, though to a slightly lesser extent than EE2/TNC. These in vivo data are in full agreement with the cell-based and biophysical assays reported above. As a whole, they provide support for the notion that compounds acting as poor activators when used separately can show increased binding capacity for PXR in the presence of

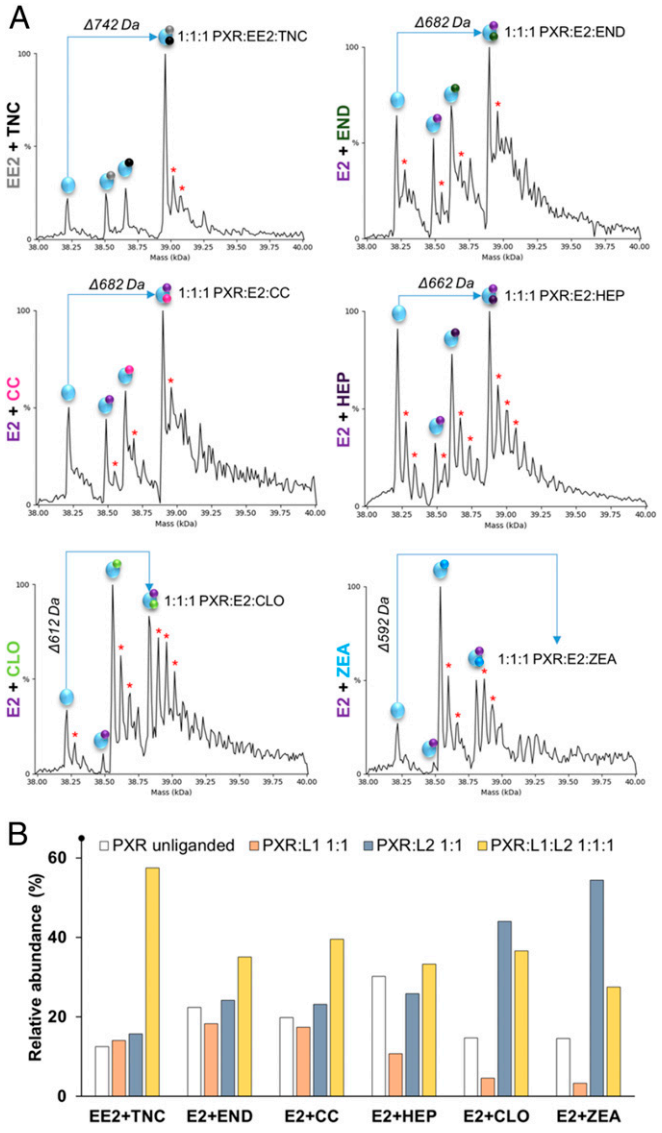

Fig. 4. Analysis of ligand-binding cooperativity by native MS. (*A*) Native ESI-MS was used to characterize PXR LBD in the presence of six binary mixtures as indicated. Asterisks indicate acetate adducts. (*B*) Relative abundance distributions of unliganded and liganded PXR (L1, EE2 or E2; L2, TNC, END, CC, HEP, CLO, or ZEA) derived from native MS analyses of PXR LBD (5 μM) in the presence of 2 molar equivalents of EE2/TNC, E2/END, E2/CC, E2/HEP, E2/CLO, and E2/ZEA ligand mixtures (10 μM each).

another ligand, thus leading to PXR activation with various degrees of synergy.

Structural Analysis of PXR LBD Bound to Composite Ligands. To gain structure-based insights into the mode of binding of the various mixtures to PXR, we solved the crystal structures of PXR LBD in complex with E2/HEP, E2/CC, E2/END, E2/CLO, and E2/ZEA at 2.50-Å, 2.15-Å, 2.0-Å, 2.3-Å, and 2.25-Å resolution, respectively (*SI Appendix*, Table S1). As for the individual ligands, all of the structures display the canonical active conformation, and, with the exception of E2 in the PXR/E2/ZEA complex, all of the ligands could be positioned unequivocally in their respective electron density (*SI Appendix*, Fig. S10 *A–D*). In agreement with native MS data (Fig. 4), the crystallographic analysis shows that E2 and ZEA are essentially mutually exclusive and that this is most likely due to the steric hindrance of M243 residing between the two compounds (*SI Appendix*, Fig. S10*E*). Fig. 6 displays the four ternary complexes for which a reliable structure could be solved. It shows that the E2 binding mode remains essentially unchanged with the 3-hydroxyl group on the A-ring forming a hydrogen bond with S247 and the 17β-hydroxyl group on the D-ring hydrogen-bonded with R410 (*SI Appendix*, Fig. S7*B*). Interestingly, while the four partner ligands remain anchored to their primary binding site (i.e., the aromatic cage), two of them, namely CC and CLO, adopt a different position from that observed in the absence of E2 (Fig. 6, *Insets*), indicating that the compounds had to modify their binding mode in order to adapt themselves to the presence of the steroidal ligand (Fig. 6 *A* and *D*). Only a slight shift was observed in the case of END (Fig. 6*C*), while HEP could not be reliably modeled in the structure of the binary complex PXR/HEP due to a poorly defined electron density, which likely reflects high mobility of this ligand when E2 is absent. A similar observation was made with TNC, which could be positioned in the ternary complex with EE2 only (8).

In line with our previous study on the EE2/TNC mixture (8), the transactivation assays reported in Fig. 1 *B–D* show that the synergism observed with certain ligand combinations relies on a gain of binding affinity of the compounds when they are coadministered. A shift of the activation curves toward the lower ligand concentrations clearly reflects this cooperative binding. We therefore performed a detailed analysis of the ternary complex structures in our hands to unveil the structural determinants of cooperative binding and affinity enhancement. Surprisingly, we found that the number and strength of interligand contacts are not correlated with the level of synergism. *SI Appendix*, Table S4*A*, reports the number of interligand interactions according to their distance as measured in the five complex structures. It shows that CLO displays the weakest synergy factor and is involved in many more interactions with the steroid than the other compounds. For instance, with only one weak contact of 4.38 Å in length, END and E2 bind cooperatively with an SF of 4.9, while the most synergistic combination EE2/TNC shows only three interactions between 3.80 Å and 4.40 Å. On the receptor side, and in the case of E2/CC and E2/END, we did not notice drastic structural changes when comparing the corresponding binary and ternary complex structures (PXR/E2, PXR/CC, and PXR/END with PXR/E2/CC and PXR/E2/END). However, we found that the interactions between the protein and a given ligand vary according to the presence or absence of the cobinder (*SI Appendix*, Table S4*B*). These variations arise from the large (CC) or slight (END, E2) repositioning of the ligands and some side-chain rearrangements upon binding of the second ligand. However, opposite situations were observed for each compound. Whereas the PXR–E2 contact count decreases in the presence of CC or END (note, however, that the two hydrogen bonds maintaining E2 are conserved in all complexes), those of PXR–CC and PXR–END remain almost constant or increase, respectively, upon E2 binding. Regarding the E2/CLO couple, which does not form a synergistic association, the structure shows a significant rearrangement of the loop following H2′ (especially around L209; *SI Appendix*, Fig. S11) accompanied by a loss of interactions of both ligands with the receptor (*SI Appendix*, Table S4*B*). As the PXR–ligand interactions largely supersede the E2–CLO contacts both in number and intensity (i.e., proximity), it is likely that a significant decrease in receptor–ligand contacts may negatively compensate the gain in stability generated by the E2/CLO interface.

This structural analysis suggests that cobinding and synergism do not follow specific rules and are therefore difficult to predict. It appears that cobinding depends on the extent to which the ligands and PXR can adapt to each other through ligand repositioning and structural rearrangement of the LBP, whereas the degree of synergism is the result of the balance between the gain and loss of stabilizing interactions occurring during formation of

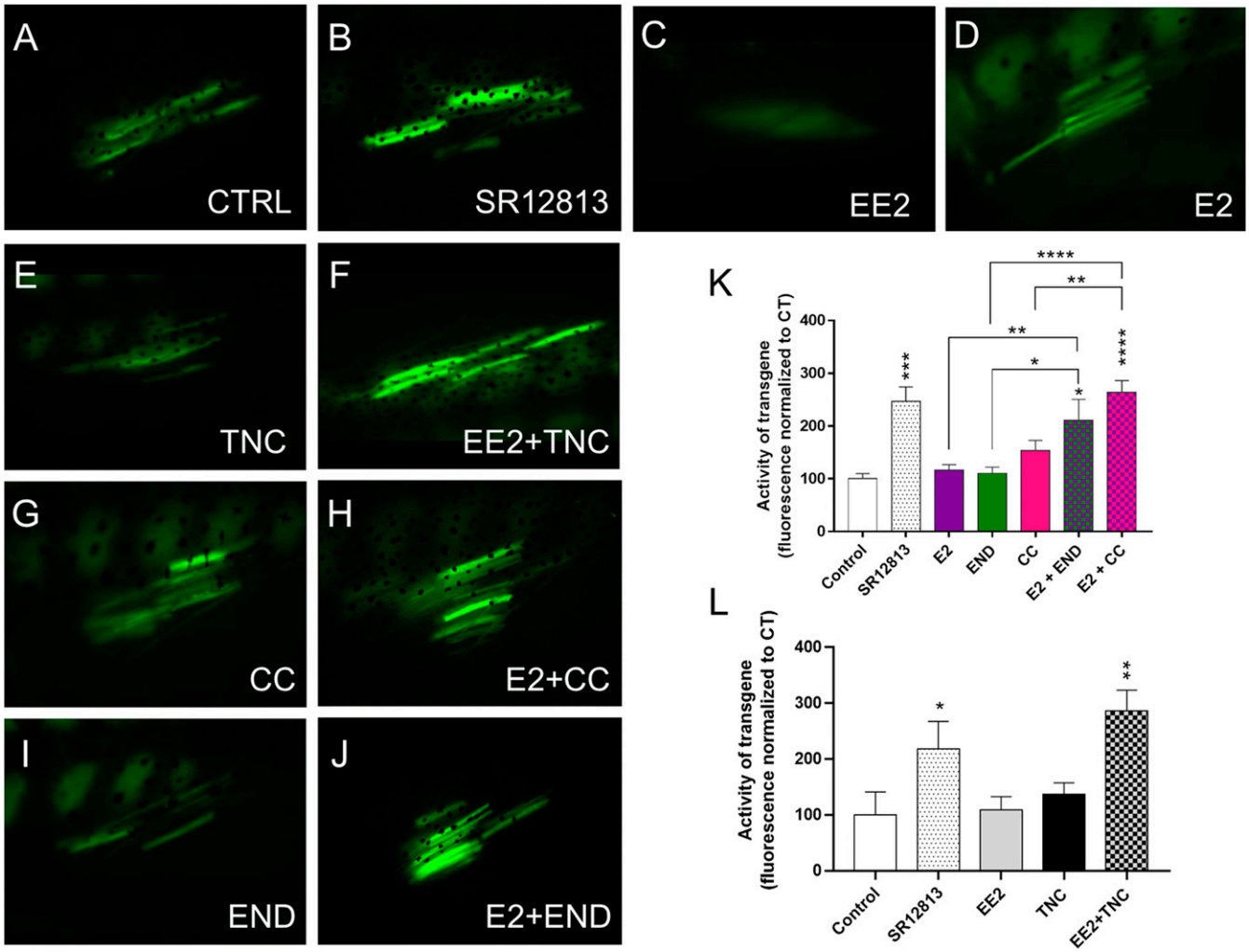

Fig. 5. PXR-driven transactivation is synergistically activated in vivo. Transient transactivation of human PXR LBD. Somatic transgenesis in tadpole tail muscle of two GFP–reporter constructs (CMV-Gal4 DBD-PXR LBD + 5UAS-GFP) was done at day 0. After 8 d of treatment with daily renewal, GFP expression was measured from pictures using ImageJ. (*A–J*) Magnification (40×) of representative tail skeletal muscle fibers (one per group) after treatment with (*A*) solvent, (*B*) PXR synthetic agonist SR12813 1 μM, (*C*) 17α-ethinylestradiol EE2 1 μM, (*D*) 17β-estradiol E2 1 μM, (*E*) TNC 1 μM, (*F*) TNC + EE2 1 μM each, (*G*) CC 0.1 μM, (*H*) E2 1 μM + CC 0.1 μM, (*I*) END 5 nM, and (*J*) E2 1 μM + END 5 nM. (*K* and *L*) Quantification of fluorescence and statistical analysis. Experiments were performed at least three times ($n > 8$ for each condition), providing similar results (*$P < 0.05$, **$P < 0.01$, ***$P < 0.001$, ****$P < 0.0001$).

the ternary complex. The weak interligand contacts displayed by synergistic couples also suggest that the mere presence of a second compound may provide a mutual stabilization by restricting ligand mobility, as seen with the EE2/TNC and E2/HEP couples for which the singly bound structures could not be determined due to TNC and HEP dynamics. These reduced dynamics would lead to a longer residence time inside the cavity and to enhanced apparent dissociation constant of the composite ligand.

Synergism through the RXR–PXR Heterodimer. The fact that PXR and RXR are heterodimerization partners raises the question whether combinations of PXR and RXR activators may cause synergistic effects. TBT is a potent environmental ligand of RXR (15, 16) responsible for a wide variety of deleterious effects in the marine ecosystem (17) and metabolic disorders in humans (18, 19). Initial experiments in colon LS174T carcinoma cells containing the full-length PXR and the CYP3A4-XREM luciferase reporter plasmid were performed to characterize the modifying effect of TBT on EE2/TNC-mediated activation of RXR–PXR. We first confirmed that EE2 and TNC act as poor RXR–PXR agonists when used separately, whereas their combination triggers a much stronger activation (Fig. 7*A*). TBT alone also acted as a poor activator of the RXR–PXR heterodimer (note that concentrations above 0.1 μM could not be used due to toxicity issues), but cotreatment with EE2 and TNC led to a shift of the activation curve of the EE2/TNC binary mixture toward better potency and efficacy values and to a strong synergistic PXR activation. This is illustrated by the theoretical activity curve obtained for the additive combination of TBT, EE2, and TNC individual activities [dashed line calculated using the Bliss independence model (20) in Fig. 7*A*]. We then compared the ability of EE2, TNC, and TBT alone or in combination to increase *CYP3A4* gene expression in LS174T cells. Consistent with the reporter gene assays, we found that EE2 and TNC cotreatment yielded much stronger activation and that the effectiveness of the binary mixture was drastically enhanced when used in combination with TBT, which, on its own, appears as a poor activator of *CYP3A4* gene expression (Fig. 7*B*).

Last, we characterized the impact of the presence of TBT on the EE2/TNC-induced coactivator recruitment by RXR–PXR. For this purpose, we used fluorescence anisotropy assays with the

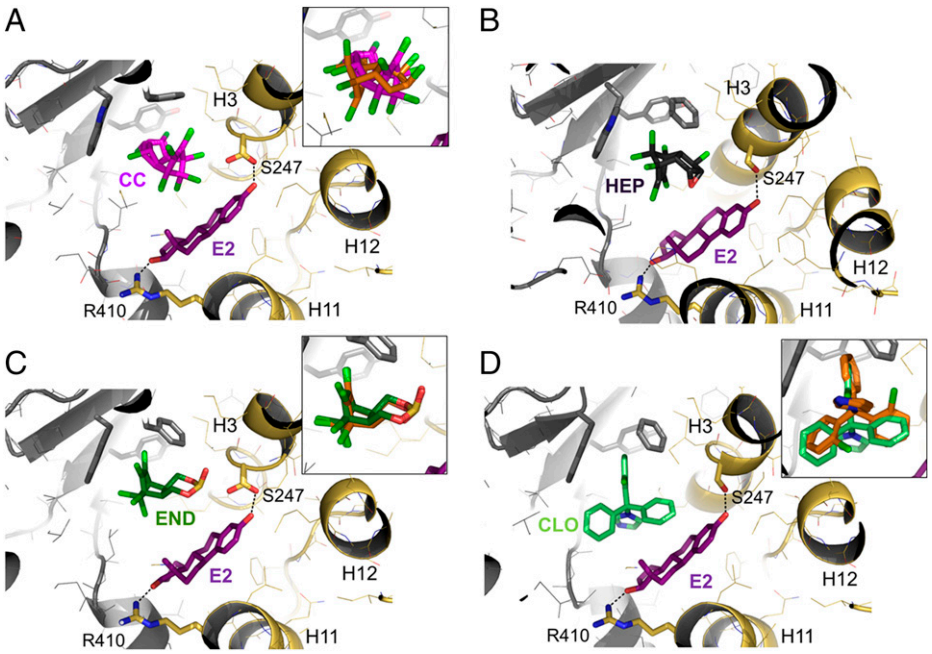

Fig. 6. The binding modes of binary mixtures as revealed by X-ray crystallography. Close-up view of the LBP of PXR bound to 17β-estradiol (E2) and (*A*) CC, (*B*) HEP, (*C*) END, and (*D*) CLO. The compounds (color code for carbon atoms as in Fig. 1*A*) and residues belonging to the aromatic cage (gray) are shown as sticks. Other residues are displayed as lines. Oxygen, nitrogen, sulfur, and chlorine atoms are colored in red, blue, yellow, and green, respectively. Residues and secondary structural elements discussed in the text are labeled. (*Insets*) Comparison of the binding modes of CC, END, and CLO in the presence and absence of E2.

purified RXR–PXR LBD heterodimer and the fluorescein-labeled NR interaction domain (NID) of SRC-1 containing three LxxLL interaction motifs. In a first step, we measured the affinity of the interaction between the heterodimer and SRC-1 NID in the presence of reference ligands and the test compounds individually. As expected, we found that the PXR agonist SR12813 efficiently enhanced SRC-1 recruitment, while the RXR agonist CD3254 induced a modest increase of the affinity of the coactivator for RXR–PXR (Fig. 7*C*). In agreement with our previous observations (8), EE2 and TNC alone had weak effects, but their combination produced a strong increase in SRC-1 recruitment, similar to that observed with SR12813. We next evaluated the effect of TBT alone and in combination. As a ligand of both RXR and PXR, TBT enhanced the affinity of the heterodimer for the coactivator with an efficiency intermediate between those of SR12813 and CD3254. We then observed that, when coincubated with TBT, the recruitment of SRC-1 induced by TNC or EE2 was increased to a level similar to that obtained

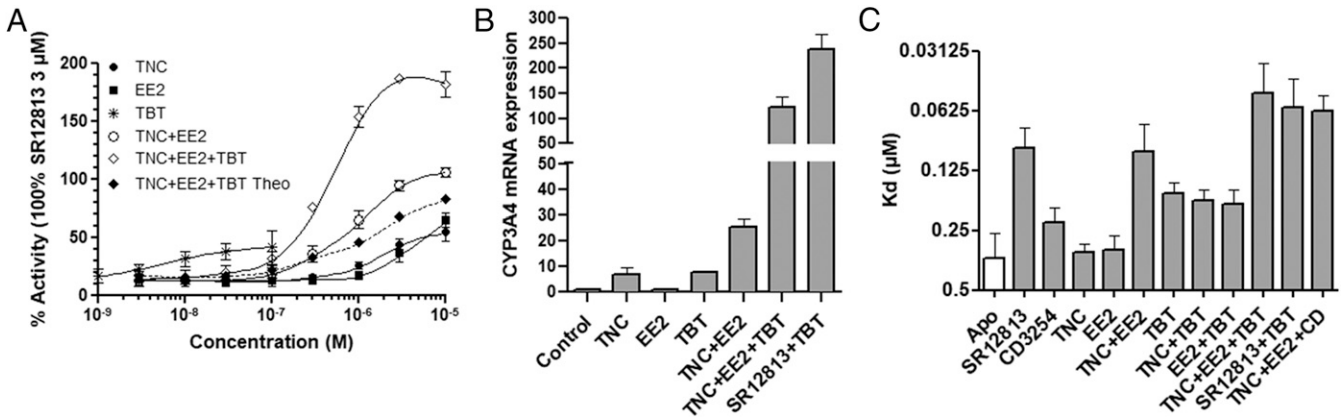

Fig. 7. Synergistic activation of the RXR–PXR heterodimer by mixtures of RXR and PXR ligands. (*A*) LS174T-PXR 3A4 luciferase cells were treated by compounds either alone or in combination as indicated. Assays were performed in triplicate in at least three independent experiments, and data are expressed as mean (±SEM). The black dashed line represents the theoretical activation curve obtained for the additive combination of EE2, TNC, and TBT activities calculated using the Bliss independence model (20). Note that, in the EE2/TNC/TBT combination, TBT is 100-fold less concentrated than EE2 and TNC. (*B*) RT-qPCR analysis of CYP3A4 mRNA expression in control or PXR-overexpressing LS174T cells treated for 48 h by solvent (0.1% DMSO) or the indicated ligands (TNC, EE2, and SR12813 at 3 µM; TBT at 30 nM). Results were obtained from three separate experiments performed in duplicates. Data are expressed as mean (±SEM) compared to DMSO-treated cells. (*C*) Fluorescence anisotropy analysis showing the relative affinity of the fluorescein-labeled SRC-1 NID for RXR–PXR LBD heterodimer in the presence of saturating concentrations of reference and test compounds alone or in mixture.

with TBT alone. However, in this case, we cannot rule out that, due to the low affinity of EE2 and TNC alone, and the competition with TBT for PXR, the measured affinity reflects TBT binding only. More importantly, we found that the strong effect of the EE2/TNC mixture on coactivator recruitment was markedly greater in the presence of TBT. Similar results were obtained when TBT was associated with the PXR agonist SR12813 or when TNC and EE2 were used in combination with the RXR agonist CD3254, demonstrating that activation of both receptors leads to the cooperative recruitment of SRC-1 to RXR–PXR via the generation of one binding site for the LxxLL motifs of coactivators on each subunit of the heterodimer. Taken together, these data support the notion that full synergistic activation of the RXR–PXR heterodimer by EDC mixtures can be attained via the combined action of two cooperative binding events involving: 1) the simultaneous interaction of two (or more) chemicals stabilizing each other within the LBP of PXR, and 2) binding of a third compound to RXR, expanding the interaction surface on the heterodimer and enhancing its affinity for transcriptional coactivators.

Concluding Remarks

In this study, we identified several PXR LBP subpockets that can accommodate small environmental ligands of diverse chemical structures due to their specific features, including a unique F/W/Y triad forming an aromatic π-trap deeply buried at the bottom of the LBP, two reactive cysteine residues available for covalent coupling, or highly malleable and adaptive secondary structural elements. These observations further substantiate the ligand-binding promiscuity of PXR and its role as a sensor responding to a wide variety of chemicals. In this respect, one can note that, while binding to different subpockets and therefore stabilizing different regions of the LBP, all compounds act as PXR agonists, differing only by their binding affinity. No specific interaction, such as, for example, with the AF-2 helix, appears required to activate the receptor. For instance, OXA and PRE, which make very little or no interaction with helix H12, serve as potent agonists, whereas E2 that is engaged in many contacts with the activation helix appears as a poor PXR activator. Nevertheless, our fluorescence anisotropy study reveals a clear direct effect of ligand binding on the recruitment of coactivators in the context of the RXR–PXR heterodimer, suggesting that ligand-dependent PXR activation involves regulatory regions of the LBD that still remain to be identified.

Our efforts to characterize novel synergistic mixtures by association of compounds for which the binding modes were pre-characterized led to the identification of four binary mixtures displaying various degrees of synergistic activity and composed of E2 (ligand group 4) as the common component and compounds bound to the organochlorine pesticides binding site (ligand group 1). In contrast, mixtures encompassing compounds from groups 2 or 3 displayed no or very weak synergistic activity. This failure is probably attributable to the very small set of compounds used in the present study. A similar strategy using high-throughput screening of large compound libraries would lead to the identification of a greater number of substances synergizing with each of the groups of ligands defined in the present study. Nonetheless, our investigations on the newly discovered mixtures reveal that: 1) cobinding does not automatically engender synergistic activity, as illustrated by the E2/CLO association; and, 2) in line with our previous results (8), the synergism observed with certain combinations results from a cooperative binding mechanism where each compound stabilizes the other, thereby leading to a global increase of their affinity for the receptor. Taken together, the results clearly show that stabilization of a compound within the LBP upon binding of a second ligand is not necessarily driven by newly created interligand contacts, but may arise from an increase in protein–ligand interactions following ligand and/or receptor rearrangement. Whether cobinding could lead to antagonism has not been observed experimentally yet, and future studies are needed to explore this possibility. Like synergism, such antagonistic effects would have major implications for both endobiotic and xenobiotic metabolism. However, PXR has proven very difficult to antagonize, and the first fully validated competitive inhibitor has been reported only recently (21). Unfortunately, the molecular details of its mode of action, in particular its impact on PXR structure and dynamics, remain vaguely understood. Some of the specific structural features of PXR LBP (e.g., large size, high plasticity) most likely account for such refractoriness to antagonism and could explain why, in our

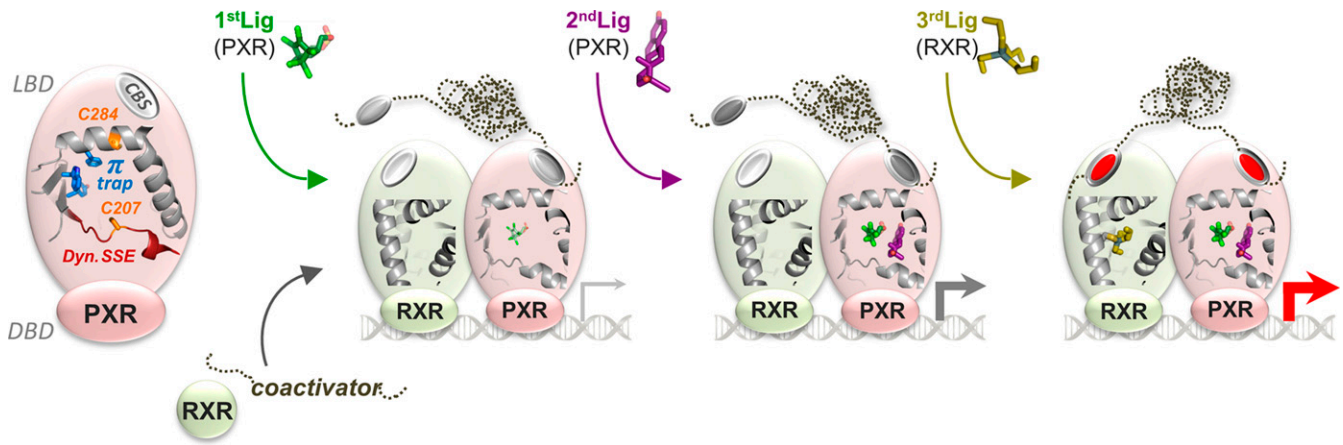

Fig. 8. Model for synergistic activation of the PXR signaling pathway by ternary mixtures of EDCs. Together with previous ones, our study shows that the LBP of PXR displays several specific structural features accounting for its role as a sensor responding to a wide variety of chemicals. They comprise an aromatic π-trap (π trap), two reactive cysteine residues (C207, C284) available for covalent coupling or highly dynamic and conformable secondary structural elements (Dyn. SSE). Upon binding of an environmental ligand to PXR, transcriptional coactivators are recruited by the DNA-bound RXR–PXR heterodimer via the interaction of one of their LxxLL binding motifs (gray ovals) with the coactivator binding site (CBS) of PXR, thus inducing the transcription of target genes. However, rather than single molecules, human exposure involves a broad mix of chemicals, which may act in a synergistic manner, possibly through the two converging mechanisms identified in this work. Both rely on the binding cooperativity of: 1) a second compound that physically assembles with the first one into the PXR LBP to form a supramolecular ligand with improved functional properties in regard to those of its individual components, or 2) a second coactivator LxxLL motif upon RXR activation insuring a robust interaction of the coactivator with the RXR–PXR heterodimer (highlighted by red ovals).

experiments, both single and double binding led to activation rather than inhibition.

Like many other NRs, PXR functions as a heterodimer with RXR whose activity can be modulated by a number of natural, synthetic, and environmental compounds (15, 22–24). Here we show that RXR (e.g., TBT) and PXR (e.g., EE2/TNC) environmental ligands can act in a concerted manner to induce cooperative recruitment of the coactivator SRC-1 by the heterodimer and the synergistic activation of RXR–PXR target gene expression. Considering the huge diversity of environmental chemicals, the mechanisms we report here for PXR are very likely to apply to other NRs, notably the peroxisome proliferator-activated receptors (PPARα, β, γ), the farnesoid receptor (FXR), or the liver X receptors (LXRα, β), which all harbor a sizable LBP and function as RXR heterodimeric partners (25). As schematized in Fig. 8, our study reports on PXR's unique features and discloses two converging cooperative binding mechanisms by which EDC mixtures can efficiently mobilize the PXR and possibly other NR pathways at much lower concentrations than those required for the individual compounds to produce similar responses. Our findings may have broad-reaching implications in the fields of toxicology, endocrine disruption, and risk assessment, and point out the need to consider chemical exposure beyond regulatory framework boundaries. In addition, many prescription drugs are known to act as low-affinity PXR ligands mediating drug–drug interactions. However, in vivo and clinical studies never take into account the combined action of coadministered pharmaceuticals that may function synergistically, thereby exacerbating PXR-dependent harmful effects. Evaluating the impact of mixed therapeutic molecules on PXR activity could help explain certain known drug interactions and perhaps reveal new ones.

Materials and Methods

Ligands. SR12813 and CD3254 were purchased from Tocris Bioscience. All of the other chemicals were purchased from Sigma-Aldrich. All compound stock solutions were prepared at 10 mM in dimethyl sulfoxide (DMSO).

Cell Lines. HG5LN GAL4-PXR and LS174T-PXR 3A4 luciferase reporter cell lines were previously described (8). They were grown in Dulbecco's modified Eagle medium (Invitrogen) supplemented with 10% fetal calf serum, L-glutamine, and antibiotics (Invitrogen).

Transactivation Assays. HG5LN GAL4-PXR and LS174T-PXR 3A4 luciferase reporter cell lines were seeded at a density of 25,000 cells per well in 96-well white opaque tissue culture plates (Greiner CellStar). Compounds to be tested were added 24 h later, and cells were incubated at 37 °C for 16 h. At the end of the incubation period, culture medium was replaced with medium containing 0.3 mM luciferin. Luciferase activity was measured for 2 s in intact living cells using a plate reader (PerkinElmer Luminometer). EC_{50} values were measured using GraphPad Prism (GraphPad Software).

PXR Crystal Structures. The human PXR LBD (residues 130 to 434) was coproduced with a fragment of the steroid receptor coactivator-1 (SRC-1, 623-710) to enhance PXR stability and purified as previously described (8). Crystals of the PXR LBD complexes were obtained by mixing 1 μL of protein (4 mg/mL) preincubated (1 h) with ligand (3 molar equivalents with 1 ligand or 1.5 each for 2 ligands) and 1 μL of precipitant [50 to 100 mM imidazole, pH 7.0 to 7.4, 8 to 14% (vol/vol) isopropanol] and equilibrated against a reservoir of 500 μL of precipitant. Crystals appeared in 24 to 48 h. Diffraction data were collected on the ID23-1, ID23-2, ID29, ID30A-1, or ID30B beamlines at the European Synchrotron Radiation Facilities (Grenoble, France) and on the PX1 beamline at the Swiss Light Source (Villigen, Switzerland). Data were processed and scaled with XDS and XSCALE (26). Crystals belong to space group $P4_32_12$. The structure was solved and refined using Phenix (13) and COOT (27). Data collection and refinement statistics are summarized in *SI Appendix*, Table S1. Figures were prepared with PyMOL (https://pymol.org/2/).

ESI-MS Analyses. Denaturing MS experiments were carried out on an electrospray time-of-flight mass spectrometer (LCT; Waters) coupled to an automated chip-based nanoelectrospray source (Triversa Nanomate; Advion Biosciences) operating in the positive ion mode. First, purified PXR LBD was buffer-exchanged against 150 mM, pH 8.0, ammonium acetate buffer (Sigma) using 0.5-mL Zeba Spin desalting columns (Thermo Fisher Scientific). Then, protein concentration was determined using a Nanodrop 2000 spectrophotometer (Thermo Fisher Scientific). PXR LBD was then incubated with a 10-molar excess of TBT or PRE ligands during 5 min at 20 °C at a final concentration of 20 μM (and 200 μM for each ligand, keeping 1% amount of DMSO). Prior to MS analyses, an external calibration was performed using the multiply charged ions produced by 2 mM horse heart myoglobin solution (Sigma) diluted in water/acetonitrile/formic acid (50/50/1, vol/vol) over the *m/z* range of 500 to 5,000. Samples were analyzed to a final concentration of 2 μM of PXR LBD diluted in the water/acetonitrile/formic acid solution using tuning parameters of the mass spectrometer as follows: backing pressure and cone voltage were set to 2.1 mbar and 40 V respectively, while raw data were acquired with MassLynx 4.1 (Waters).

Native MS experiments were performed on a hybrid electrospray quadrupole time-of-flight mass spectrometer (Synapt G2 HDMS; Waters) coupled to an automated chip-based nanoelectrospray source (Triversa Nanomate; Advion Biosciences) operating in the positive ion mode. PXR LBD was buffer-exchanged as described above and incubated during 5 min at 20 °C to a final concentration of 5 μM (in 150 mM NH4Ac, pH 8.0) with a 2-molar excess of binary mixtures (EE2/TNC, E2/END, E2/CC, E2/HEP, E2/CLO, or E2/ZEA; 10 μM each). Prior to analyses, mass spectrometer calibration was performed using singly charged ions produced by a 2-mg/mL solution of cesium iodide in 2-propanol/water (1v/1v; Sigma) over the *m/z* range 1,000 to 10,000. Instrumental parameters were optimized to get an optimal *m/z* ion transmission without dissociation of weak noncovalent interactions by raising the backing pressure, the cone voltage, and the extraction voltage to 6 mbar, 20 V, and 5 V, respectively (acquisition performed with MassLynx 4.1).

Deconvolution of MS spectra was performed using UniDec version 4.1.2 (28) using the following parameters: *m/z* ranges were set to 1,000 to 1,700 and to 3,100 to 4,100 for denaturing and native MS experiments, respectively. Processing parameters were set as follows: substract curved, 10; normalize data, nonlinear; sample mass every 10 Da; charge range, 20 to 40 and 10 to 12; and mass range, 38,000 to 39,000 and 38,000 to 40,000 Da for denaturing and native MS experiments, respectively. Deconvolution parameters were set as follows: peak full width at half maximum, 0.85; charge smooth width, 1.0; point smooth width, 1.0; peak detection range, 10.0 Da; and peak detection threshold, 0.15. Relative abundance described in Fig. 4*B* was calculated from the intensities given by UniDec for the four considered species: PXR unliganded, PXR:L1, PXR:L2, and PXR:L1:L2.

Steady-State Fluorescence Anisotropy. The RXR–PXR LBD heterodimer and the fluorescein-labeled SRC-1 NID were prepared as previously described (8). Measures of the binding affinities of the coactivator fragment for the heterodimer in the absence and presence of various ligands were performed using a Safire2 microplate reader (TECAN). The excitation wavelength was set at 470 nm, and emission measured at 530 nm for the fluorescein-tagged fragment. Assays were carried out in the following buffer solution: 20 mM Tris·HCl, pH 7.5, 150 mM NaCl, 1 mM tris(2-carboxyethyl)phosphine, and 5% (vol/vol) glycerol. We initiated the measurements at the highest concentration of protein (20 μM) and diluted the protein sample twofold successively with the buffer solution. For each point of the titration curve, the protein sample was mixed with 5 nM of fluorescent fragment and a 3-molar excess of ligand (60 μM final concentrations). Binding data were fitted using a sigmoidal dose–response model using GraphPad Prism (GraphPad Software).

RT-PCR and Real-Time qPCR. Total RNA was isolated with EXTRACTME Total RNA Kit (Blirt; cat. no. EMO9.1). One microgram of total RNA was reverse-transcribed to cDNA using the 5× All-In-One RT Master mix (Abm; cat. no. G490). qPCRs were performed using SYBR green (Qiagen) and specific primers with the LightCycler-480 real-time PCR system (Roche Diagnostics). Sequences of each primer were as follows: *Cyp3a4*, forward, 5′-GCCTGGTGCTCCTCTATCTA-3′; and reverse, 5′-GGCTGTTGACCATCATAAAAG-3′; *Actb*, forward, 5′-AGGCACCAGGGCGTGAT-3′; and reverse, 5′-GCCCACATAGGAATCCTTCTGAC-3′. The relative amount of RNA was calculated with the $2^{\Delta\Delta CT}$ method, and gene expression was normalized using β-actin.

Somatic Gene Transfer. *Xenopus* tadpoles were obtained from Centre de Ressources Biologiques Xénopes (Université Rennes 1, Unité Mixte de Service 3387) at stage Nieuwkoop-Faber (NF) 50. Animals were fed and raised until NF53 for 2 wk. A mixture of two different circular plasmids (800 ng CMV-Gal4 DBD-PXRLBD + 800 ng 5UAS-GFP, 1 μL of NaCl 0.45%) was injected into

BIOCHEMISTRY

the skeletal–dorsal muscle as previously described (29, 30). Tadpoles are anesthetized before injections in MS222 0.1%.

Treatments. After injection, tadpoles were placed for at least 1 h in clean water to let them recover. Seven different treatments were made. Each group was composed of 10 tadpoles in a glass tank of 1 L containing 0.5 L of water with chemical. Stock solutions of all compounds used were done in DMSO at 0.1 M, aliquoted at 10 μL, and stored at −20 °C until use. New aliquots were used for renewal every day for 8 d. DMSO content in all tanks was 1/5,000. We examined first the effect of SR12813 (1 μM), E2 (1 μM), END (5 nM), CC (0.1 μM), and two combinations, E2 with END and E2 with CC, and confirmed the synergistic effect of TNC+EE2 using 1 μM of each or the combination of the two compounds. The renewal of the chemical solutions was done during 7 d in the afternoon and with food added in the tank the following morning to avoid any trapping by the food.

Imaging and Fluorescence Quantification. Tadpoles were placed in MS222 0.1% until immobility, washed in clean water, and placed into a wet chamber. Images were acquired using a Leica MZ16F fluorescence stereo microscope (MZ16F) equipped with a Q.imaging retiga camera, driven by QCapture Pro-6.0 software, and an eGFP filter bandpass. All pictures were taken with the same parameters (40× objective and 600-ms exposure time, gain 4). The quantification of fluorescence was measured only in a region of interest delimited to the transfected muscle fibers using ImageJ software.

Statistical Analysis of Results. Experiments were reproduced three times following the same protocol with three different batches of animals. For each independent experiment, data from all groups were normalized to the control group (to 100 value). Then, a pool of all data was made. Graphs and statistical analysis were done using GraphPad Prism (GraphPad Software). When two groups are presented on a graph, nonparametric Mann–Whitney tests are used; for three or more groups, we used nonparametric Kruskal–Wallis tests with Dunn's multiple comparison posttest.

Data Availability. The atomic coordinates and structure factors have been deposited in the PDB under accession codes 7AX8 (apo), 7AX9 (CC), 7AXA (CLO), 7AXB (END), 7AXC (FER), 7AXD (FIP), 7AXE (OXA), 7AXF (PRE), 7AXG (TBT), 7AXH (ZEA), 7AXI (CC/E2), 7AXJ (CLO/E2), 7AXK (END/E2), and 7AXL (HEP/E2).

ACKNOWLEDGMENTS. We acknowledge experimental assistance from the staff of the European Synchrotron Radiation Facility (Grenoble, France) during data collection. We acknowledge financial support from the Agence Nationale de la Recherche (ANR), projects SYNERACT (to P. Balaguer and W.B.) and TOXSYN (to B.D., J.-B.F., P. Balaguer, and W.B.), Plan Cancer INSERM project SYNERPXR 2.0 (to P. Balaguer and W.B.), and the French Agency for Food, Environmental and Occupational Health & Safety projects XENOMIX (to P. Balaguer and W.B.) and TOXCHEM (to P. Balaguer and W.B.). This project has received funding from the European Union's Horizon 2020 research and innovation program under Grant Agreements No. 825489 (to P. Balaguer and W.B.), No. 825759, and No. 825161 (to J.-B.F. and B.D.). Centre de Biologie Structurale is a member of France-BioImaging and the French Infrastructure for Integrated Structural Biology. Laboratoire de Spectrométrie de Masse BioOrganique (LSMBO) is part of the French Proteomic Infrastructure, three national infrastructures supported by the French National Research Agency (ANR-10-INBS-04-01, ANR-10-INBS-05, and ANR-10-INBS-08-03, respectively). The LSMBO would like to thank Groupement d'Intérêt Scientifique Infrastrutures en Biologie Sante et Agronomie and Région Alsace for financial support in purchasing a Synapt G2 HDMS instrument.

1. J. Yan, W. Xie, A brief history of the discovery of PXR and CAR as xenobiotic receptors. *Acta Pharm. Sin. B* **6**, 450–452 (2016).
2. T. M. Willson, S. A. Kliewer, PXR, CAR and drug metabolism. *Nat. Rev. Drug Discov.* **1**, 259–266 (2002).
3. P. O. Oladimeji, T. Chen, PXR: More than just a master xenobiotic receptor. *Mol. Pharmacol.* **93**, 119–127 (2018).
4. H. Wang *et al*., Pregnane X receptor activation induces FGF19-dependent tumor aggressiveness in humans and mice. *J. Clin. Invest.* **121**, 3220–3232 (2011).
5. Y. Sui *et al*., Bisphenol A increases atherosclerosis in pregnane X receptor-humanized ApoE deficient mice. *J. Am. Heart Assoc.* **3**, e000492 (2014).
6. N. K. Chaturvedi, S. Kumar, S. Negi, R. K. Tyagi, Endocrine disruptors provoke differential modulatory responses on androgen receptor and pregnane and xenobiotic receptor: Potential implications in metabolic disorders. *Mol. Cell. Biochem.* **345**, 291–308 (2010).
7. S. C. Chai, M. T. Cherian, Y. M. Wang, T. Chen, Small-molecule modulators of PXR and CAR. *Biochim. Biophys. Acta* **1859**, 1141–1154 (2016).
8. V. Delfosse *et al*., Synergistic activation of human pregnane X receptor by binary cocktails of pharmaceutical and environmental compounds. *Nat. Commun.* **6**, 8089 (2015).
9. R. Altenburger *et al*., Mixture effects in samples of multiple contaminants–An inter-laboratory study with manifold bioassays. *Environ. Int.* **114**, 95–106 (2018).
10. O. V. Martin, R. M. Evans, M. Faust, A. Kortenkamp, A human mixture risk assessment for neurodevelopmental toxicity associated with polybrominated diphenyl ethers used as flame retardants. *Environ. Health Perspect.* **125**, 087016 (2017).
11. A. Kortenkamp, Low dose mixture effects of endocrine disrupters and their implications for regulatory thresholds in chemical risk assessment. *Curr. Opin. Pharmacol.* **19**, 105–111 (2014).
12. A. Kortenkamp, Low dose mixture effects of endocrine disrupters: Implications for risk assessment and epidemiology. *Int. J. Androl.* **31**, 233–240 (2008).
13. P. D. Adams *et al*., PHENIX: A comprehensive python-based system for macromolecular structure solution. *Acta Crystallogr. D Biol. Crystallogr.* **66**, 213–221 (2010).
14. Y. Xue *et al*., Crystal structure of the pregnane X receptor-estradiol complex provides insights into endobiotic recognition. *Mol. Endocrinol.* **21**, 1028–1038 (2007).
15. A. le Maire *et al*., Activation of RXR-PPAR heterodimers by organotin environmental endocrine disruptors. *EMBO Rep.* **10**, 367–373 (2009).
16. F. Grün *et al*., Endocrine-disrupting organotin compounds are potent inducers of adipogenesis in vertebrates. *Mol. Endocrinol.* **20**, 2141–2155 (2006).
17. B. G. McAllister, D. E. Kime, Early life exposure to environmental levels of the aromatase inhibitor tributyltin causes masculinisation and irreversible sperm damage in zebrafish (Danio rerio). *Aquat. Toxicol.* **65**, 309–316 (2003).
18. F. Grün, B. Blumberg, Endocrine disrupters as obesogens. *Mol. Cell. Endocrinol.* **304**, 19–29 (2009).
19. R. J. Egusquiza, B. Blumberg, Environmental obesogens and their impact on susceptibility to obesity: New mechanisms and chemicals. *Endocrinology* **161**, bqaa024 (2020).
20. W. Zhao *et al*., A new Bliss independence model to analyze drug combination data. *J. Biomol. Screen.* **19**, 817–821 (2014).
21. W. Lin *et al*., SPA70 is a potent antagonist of human pregnane X receptor. *Nat. Commun.* **8**, 741 (2017).
22. M. Dominguez, S. Alvarez, A. R. de Lera, Natural and structure-based RXR ligand scaffolds and their functions. *Curr. Top. Med. Chem.* **17**, 631–662 (2017).
23. P. García, P. Lorenzo, A. R. de Lera, Natural ligands of RXR receptors. *Methods Enzymol.* **637**, 209–234 (2020).
24. A. le Maire, W. Bourguet, P. Balaguer, A structural view of nuclear hormone receptor: Endocrine disruptor interactions. *Cell. Mol. Life Sci.* **67**, 1219–1237 (2010).
25. N. Gallastegui, J. A. Mackinnon, R. J. Fletterick, E. Estébanez-Perpiñá, Advances in our structural understanding of orphan nuclear receptors. *Trends Biochem. Sci.* **40**, 25–35 (2015).
26. W. Kabsch, Xds. *Acta Crystallogr. D Biol. Crystallogr.* **66**, 125–132 (2010).
27. P. Emsley, K. Cowtan, Coot: Model-building tools for molecular graphics. *Acta Crystallogr. D Biol. Crystallogr.* **60**, 2126–2132 (2004).
28. M. T. Marty *et al*., Bayesian deconvolution of mass and ion mobility spectra: From binary interactions to polydisperse ensembles. *Anal. Chem.* **87**, 4370–4376 (2015).
29. A. de Luze, L. Sachs, B. Demeneix, Thyroid hormone-dependent transcriptional regulation of exogenous genes transferred into Xenopus tadpole muscle in vivo. *Proc. Natl. Acad. Sci. U.S.A.* **90**, 7322–7326 (1993).
30. L. Coen, K. Kissa, S. le Mevel, P. Brulet, B. A. Demeneix, A somatic gene transfer approach using recombinant fusion proteins to map muscle-motoneuron projections in Xenopus spinal cord. *Int. J. Dev. Biol.* **43**, 823–830 (1999).